

Quantum wires in magnetic field: A comparative study of the Hartree-Fock and the spin density functional approaches

S. Ihnatsenka and I. V. Zozoulenko

*Solid State Electronics, Department of Science and Technology (ITN),
Linköping University, 60174 Norrköping, Sweden*

(Dated: November 30, 2018)

We present a detailed comparison of the self-consistent calculations based on the Hartree-Fock and the spin density functional theory for a spit-gate quantum wire in the IQH regime. We demonstrate that both approaches provide qualitatively (and in most cases quantitatively) similar results for the spin-resolved electron density, spin polarization, spatial spin separation at the edges and the effective g factor. The both approach give the same values of the magnetic fields corresponding to the successive subband depopulation and qualitatively similar evolution of the magnetosubbands. Quantitatively, however, the HF and the DFT subbands are different (even though the corresponding total electron densities are practically the same). In contrast to the HF approach, the DFT calculations predict much larger spatial spin separation near the wire edge for the low magnetic fields (when the compressible strips for spinless electrons are not formed yet). In the opposite limit of the large fields, the Hartree-Fock and the DFT approaches give very similar values for the spatial spin separation.

PACS numbers: 73.21.Hb, 73.43.Cd, 73.23.Ad

Introduction. A detailed knowledge of energetics, spin splitting, magnetosubband and edge state structure in quantum wires is necessary for understanding and interpretation of a variety of magnetotransport phenomena in the integer quantum Hall (IQH) regime. A powerful tool to study electron-electron interaction and spin effects in quantum wires is the mean-field approaches such as the Hartree-Fock (HF) and the spin density functional theory (DFT)¹. A number of studies based on these approaches addressing various aspects of interacting electrons in the IQH regime in quantum wires have been reported recently^{2,3,4,5,6,7,8,9,10,11,12,13,14,15}. However, in some cases different studies arrive to conflicting results and findings reported in some studies are not recovered in others. It is not clear whether the reason for such discrepancies is due to utilization of different approaches treating the exchange and correlation effects in different ways (i.e. HF vs spin DFT), or this difference is related to various approximations of different models (such as e.g. neglecting a global electrostatics, simplified models for screening, non self-consistent calculations, fixed filling factors, etc.).

The aim of this Brief report is to resolve this issue by presenting a detailed comparison of the self-consistent calculations based on the HF method and the spin DFT approximation for a spit-gate quantum wire in the IQH regime. This includes a comparison of the magnetosubband structure, electron densities, spin polarization and spatial spin separation as well as calculation of the effective g factor. We stress that in our calculations we do not use any simplified assumptions concerning screening such that a global electrostatics of the system at hand is treated in an exact way. Note that comparative studies of different approaches are common in treatment of electronic properties of quantum dots as they provide an important insight into the validity of applied methods

and used approximations¹⁶. At the same time, we are not aware of corresponding studies for the quantum wires in the IQH regime. Another motivation for the present study is that the DFT based approaches are often used for transport calculations. It has been argued recently that the standard DFT approaches might not be always suitable for this purpose (notably in the weak coupling regime), because of the inherent problems of the derivative discontinuity problem and related uncompensated self-interaction errors in the DFT¹⁷. At the same time, the HF approach does not suffer from the above problems and thus the utilization of the HF method in the transport calculations overcomes the limitations of the standard DFT. Thus, the detailed comparison of these two methods can provide a justification for the utilization of the HF instead of the DFT.

Basics We consider an infinitely long split-gate GaAs/AlGaAs quantum wire in a perpendicular magnetic field B where electrons are situated at the distance b below the surface. The HF equation for a single-particle wave function of spin σ , $\Phi_\beta^\sigma(\mathbf{r})$, reads¹

$$[H_0(\mathbf{r}) + V_{conf}(y) + V_H(y) + V_Z] \Phi_\beta^\sigma(\mathbf{r}) + \int V_{Fock}(\mathbf{r}, \mathbf{r}') \Phi_\beta(\mathbf{r}') d\mathbf{r}' = E_\beta \Phi_\beta^\sigma(\mathbf{r}), \quad (1)$$

where $\mathbf{r} = (x, y)$, $H_0(\mathbf{r}) = -\frac{\hbar^2}{2m^*} \left(\frac{\partial}{\partial x} - \frac{eiBy}{\hbar} \right)^2 + \frac{\partial^2}{\partial y^2}$ is the kinetic energy in the Landau gauge, with $m^* = 0.067m_e$ being the GaAs effective mass; $\sigma = \pm \frac{1}{2}$ describes spin-up and spin-down states, \uparrow , \downarrow . In the split-gate geometry the bare confining potential $V_{conf}(y)$ due to the gates, donor layers and the Schottky barrier is well approximated by the parabolic confinement, $V_{conf}(y) = V_0 + \frac{m^*}{2} (\omega_0 y)^2$, where V_0 defines the bottom of the potential (we set the Fermi energy $E_F = 0$)¹³. The Zeeman energy is $V_Z = g\mu_B B \sigma$ where $\mu_B = e\hbar/2m_e$

is the Bohr magneton and the bulk g factor of GaAs is $g = -0.44$. The Hartree potential due to the electron density $n(y) = \sum_{\sigma} n^{\sigma}(y)$ (including the mirror charges) is¹³ $V_H(y) = -\frac{e^2}{4\pi\epsilon_0\epsilon_r} \int dy' n(y') \ln \frac{(y-y')^2}{(y-y')^2 + 4b^2}$. The non-local Fock operator is $V_{Fock}(\mathbf{r}, \mathbf{r}') = -\frac{e^2}{4\pi\epsilon_0|\mathbf{r}-\mathbf{r}'|} \sum_{\beta} f_{E_{\beta}}^{FD} \Phi_{\beta}^{\sigma}(\mathbf{r}) \Phi_{\beta}^{\sigma*}(\mathbf{r}')$, where the summation is performed over all states β , and $f_{E_{\beta}}^{FD}$ is the Fermi-Dirac distribution function.

We assume the Bloch form of the wave function,

$$\Phi_{n,k}^{\sigma}(x, y) = e^{ikx} \varphi_{n,k}^{\sigma}(y) \quad (2)$$

where k is the wave vector, $\varphi_{n,k}(y)^{\sigma}$ describes the n -th transverse subband for the spin σ . Substituting the Bloch function (2) into the HF equation (1) and integrating over the longitudinal coordinate x we arrive to the set of eigenequations for $\varphi_{n,k}(y)$,⁹

$$\left[-\frac{\hbar^2}{2m^*} \frac{d^2}{dy^2} + \frac{m^* \omega_c^2}{2} \left(y + \frac{\hbar k}{eB} \right)^2 + V_{conf}(y) + V_H(y) + V_Z \right] \varphi_{n,k}^{\sigma}(y) + \int V_{Fock}^k(y, y') \varphi_{n,k}^{\sigma}(y') dy' = E_{n,k}^{\sigma} \varphi_{n,k}^{\sigma}(y), \quad (3)$$

where ω_c is the cyclotron frequency and

$$V_{Fock}^k(y, y') = -\frac{e^2}{2\pi\epsilon_0\epsilon_r} \sum_{n',k'} f_{E_{n',k'}}^{FD} \varphi_{n',k'}^{\sigma}(y) \varphi_{n',k'}^{\sigma*}(y') \times K_0(|k - k'| |y - y'|), \quad (4)$$

with K_0 being the modified Bessel function. Discrediting Eq. (3) we reduce the system of the integro-differential equations to the system of linear equations, which we solve numerically by standard methods in an iterative way until the self-consistent solution is achieved. Knowledge of the wave vectors k_n^{σ} for different states $\{n, \sigma\}$ allows us to recover the subband structure¹³, i.e. to calculate an overage position y_n^{σ} of the wave functions for different modes n , $y_n^{\sigma} = \hbar k_n^{\sigma} / eB$.

Within the framework of the spin density functional theory, the Kohn-Sham equations for the single particle wave function $\Phi_{\beta}^{\sigma}(\mathbf{r})$ read

$$[H_0(\mathbf{r}) + V^{\sigma}(y)] \Phi_{\beta}^{\sigma}(\mathbf{r}) = E_{\beta} \Phi_{\beta}^{\sigma}(\mathbf{r}), \quad (5)$$

$$V^{\sigma}(y) = V_{conf}(y) + V_H(y) + V_Z + V_{xc}^{\sigma,\zeta}(y), \quad (6)$$

where the first three terms in the effective confinement potential $V^{\sigma}(y)$ are the same as in the HF equation (1), and the last term corresponds to the exchange and correlation potential in the local spin density approximation. It is given by the functional derivative $V_{xc}^{\sigma,\zeta} = \frac{\delta}{\delta n^{\sigma}} \{n \epsilon_{xc}^{\zeta}(n)\}$, where $\epsilon_{xc}^{\zeta}(n)$ is the exchange and correlation energy functional and $\zeta(y) = \frac{n^{\uparrow} - n^{\downarrow}}{n^{\uparrow} + n^{\downarrow}}$ is the local spin polarization. All the results presented below correspond to the parameterization of $\epsilon_{xc}^{\zeta}(n)$ given by Tanatar and Ceperley¹⁸. Assuming the Bloch form of

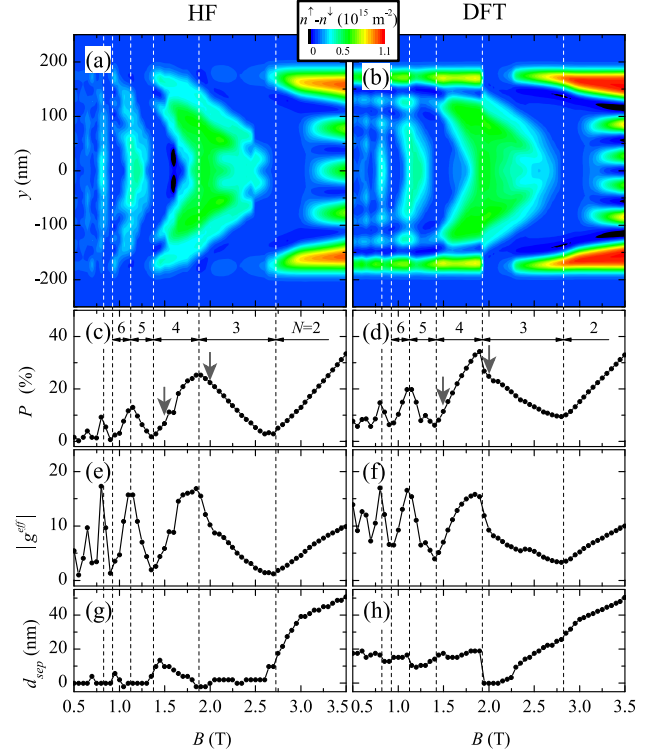


FIG. 1: (Color online). (a),(b) Spatially resolved spin polarization of the electron density $n^{\uparrow} - n^{\downarrow}$. (c),(d) The number of subbands and the total spin polarization $P = \frac{n_{1D}^{\uparrow} - n_{1D}^{\downarrow}}{n_{1D}^{\uparrow} + n_{1D}^{\downarrow}}$; arrows indicate the magnetic fields corresponding to the magnetosubband structure shown in Fig. 2; (e),(f) The effective g factor. (g),(h) The spatial spin separation at the wire edge d_{sep} (a definition of d_{sep} is outlined in Fig. 2 (a)). The left and right panels correspond respectively to the HF and the spin DFT approximations. The bare confining potential $V_{conf}(y)$ is well approximated by the parabolic confinement with $V_0 = -85\text{meV}$, $\hbar\omega_c = 2\text{meV}$, the distance to the surface $b = 60\text{nm}$, temperature $T = 1\text{K}$.

the wave functions (2), the equations (5) are solved self-consistently using the Green's function technique as described in detail in Ref. 13 (see also Refs. 14,15).

Note that we find the self-consistent solutions for the DFT and the HF approaches using completely unrelated numerical methods. As a validity check we control that these different methods give identical results when we set V_{Fock}^k and $V_{xc}^{\sigma,\zeta}$ in respectively Eqs. (3) and (6) to zero and thus reduce both approaches to the standard spinless Hartree approximation (the latter is shown to reproduce well^{14,20} the Chklovskii *et al.*¹⁹ electrostatic treatment).

Results and discussion. Figure 1 show a spatially resolved difference in the electron density $n^{\uparrow} - n^{\downarrow}$ and the total spin polarization $P = \frac{n_{1D}^{\uparrow} - n_{1D}^{\downarrow}}{n_{1D}^{\uparrow} + n_{1D}^{\downarrow}}$ calculated using the HF and the spin DFT approaches for a representative quantum wire ($n_{1D}^{\sigma} = \int n^{\sigma}(y) dy$). A detailed analysis of the spin polarization in a split-gate quantum wire based on the spin-DFT approach is given in Refs. 13,14. For

the sake of comparison with the HF approximation we summarize below the main finding. The spin polarization is maximal for magnetic fields close to the depopulation of the even subbands, see Fig. 1 (d). In this case the highest occupied (odd) subband forms a compressible strip in the middle of the wire, and, therefore, the electron density is mostly spin-polarized in the centre of the wire, see Fig. 2 (d). (We define the width of the compressible strip within the window $|E - E_F| \leq 2\pi kT$,^{13,14,15,20} which corresponds to the energy interval where the subbands are partially filled, $0 < f^{FD} < 1$). Minima of the spin polarization correspond, instead, to depopulation of the odd subbands. At polarization minima the spin-up and spin-down subbands are fully (and practically equally) occupied as their bottoms in the center of the wire are situated below (or just on the border) of the energy window $|E - E_F| \leq 2\pi kT$, see Fig. 2 (c). Because of this, the spin polarization in the centre of the wire is absent and it increases toward the edges of the wire because the spin-up and spin-down subbands intersect E_F at different distances from the wire center. For the case of spinless electrons the compressible strips are formed near the wire boundaries for sufficiently high magnetic fields^{14,19,20}. The exchange interaction, however, completely or partially suppress the compressible strips leading to a spatial spin separation between the spin-up and spin-down states¹⁴. This spatial separation causes a strong spin polarization near the boundaries which is clearly seen in Fig. 1 (b) for magnetic fields $B \gtrsim 2.75$ T. This spin separation grows as the magnetic field increases because the width of the corresponding compressible strips for the spinless electrons increases, see Figs. 1 (b), (h). Note that the spin-DFT approach also predicts an almost constant (independent of B) spatial spin polarization even for lower fields $B \lesssim 2.0$ T, when the compressible strips are not formed yet.

Let us now compare the results of the spin-DFT calculations with those based on the HF approach. It is remarkable that the both approaches give practically the same values of the magnetic fields corresponding to the successive subband depopulation, c.f. Figs. 1 (c) and (d). Moreover, both approaches give practically the same *total* electron density distribution $n(y)$, see Fig. 2 (a) and (b). However, the *spin-resolved* densities are not always the same. In contrast to the spin-DFT approach, the HF calculation does not always exhibit a spatial spin polarization near the edges for the low fields (when the compressible strips for spinless electrons are not formed yet). This is the case for a quantum wire of Fig. 1 for $B \lesssim 2.75$ T. The spin separation near the wire edges d_{sep} is caused by the exchange interaction and it is known to depend on the steepness of the confinement potential^{3,21}: as the external confining potential becomes smoother, the spin separation grows. Figure 3 shows that while the spatial spin separation d_{sep}^{DFT} and d_{sep}^{HF} exhibit qualitatively same behavior as a function of the potential steepness, the DFT approaches predicts much larger spatial spin separation as compared to the HF method. Besides, the

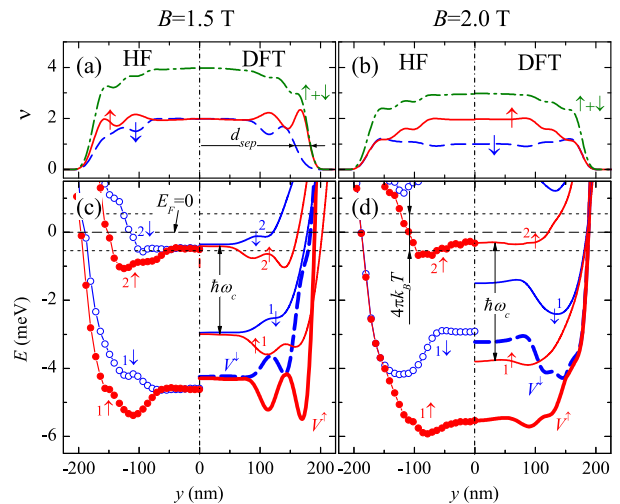


FIG. 2: (Color online). (a),(b) The local filling factors $\nu^\uparrow, \nu^\downarrow$ and $\nu = \nu^\uparrow + \nu^\downarrow$ ($\nu = nh/eB$) calculated within the HF and the spin DFT approaches for two representative magnetic fields (indicated by arrows in Fig. 1 (c),(d)). (c),(d) The magnetosubband structure for spin-up and spin-down electrons calculated within the HF and the spin DFT approaches. The fat solid lines indicate the DFT effective confinement potential V^σ , Eq. (6) (note that because of the nonlocal character of the HF equations, it is not possible to define the effective confinement potential in the HF approach.)

critical value of the potential steepness at which different spins become spatially separated is obviously lower in the HF approach. We stress that the difference between d_{sep}^{DFT} and d_{sep}^{HF} discussed above corresponds to the regime of the low fields, when the compressible strips for spinless electrons are not formed yet. For larger fields (corresponding to the formation of compressible strips for the spinless electrons), the Hartree-Fock and the DFT approaches give very similar values for the spin separa-

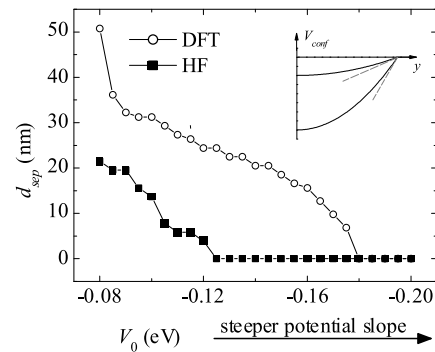


FIG. 3: The spatial spin separation near the wire edge as a function of the confinement steepness calculated within the spin DFT and HF approaches in the regime of low fields ($B = 0.5$ T). The inset illustrates how the confinement steepness changes as the bottom of the parabolic confinement potential, V_0 , varies ($\hbar\omega_0$ is adjusted to keep the wire width constant, $w = 500$ nm.)

tion, c.f. Figs. 1 (g) and (h). In this case d_{sep} is approximately equal to the width of the compressible strips for spinless electrons (see Ref. 14 for a detailed discussion of the suppression of the compressible strips by the exchange interaction leading to the spatial spin polarization at the edges). Note that our study can not distinguish which approach gives a correct result for d_{sep} for the low field. This question can be resolved by a comparison to the exact results obtained by e.g. quantum Monte Carlo methods. We speculate at this point that it is the DFT approach that overestimates the spatial spin separation at lower fields. This conclusion is based on transport measurements on lateral quantum dots indicating that the spin polarized injection and detection by means of the spatial separation of spins can be achieved only in the edge state regime for sufficiently high magnetic field²².

Let us turn our attention to the subband structure. Figure 2 shows the subband structure for two representative magnetic fields corresponding to the minimum and maximum of the spin polarization in a quantum wire. Qualitatively, the HF and the DFT subbands exhibit very similar features and evolve in a similar way as the magnetic field is changed. This includes the subband depopulation, the formation of the compressible strip in the middle of the wire and the subband separation at the edges. Quantitatively, however, the HF and the DFT subbands are different (even though the corresponding densities are practically the same, see Fig. 2 (b), (d)). The most pronounced difference is that the consecutive subband separation for different spins in the DFT approach is equal to $\hbar\omega_c$, whereas the HF subband separation exceeds this value. We attribute this difference to the nonlocal character of the exchange interaction in the HF approximation. Note that the HF subband separation tends to $\hbar\omega_c$ as the density increases because the exchange interaction becomes less pronounced for higher densities in comparison to the kinetic energy.

Because the DFT and HF approaches give rather similar evolution of the magnetosubband structure, the corresponding behavior of the total spin-polarization P and the effective g factor, g^{eff} , is also similar, see Figs. 1 (c), (d), and (e), (f). (We define the effective g factor according to $g^{eff} = \langle (E_{n,k}^\uparrow - E_{n,k}^\downarrow) / g\mu_B B \rangle$ where the averaging is performed over the all k vectors and the occupied subbands n). The DFT approach gives a slightly higher value of P at the lower fields because of the enhanced spin polarization near the edges as discussed above. The both approaches give quantitatively similar dependencies of g^{eff} as a function of magnetic field. Because g^{eff} is directly related to the subband spin splitting, the dependence of $g^{eff} = g^{eff}(B)$ closely follows that of $P = P(B)$, showing a well-known oscillatory character with a periodicity of $1/B$ related to the subband depopulation²³. A maximum value of $g^{eff} \approx 15$ is reached close to magnetic fields corresponding to depopulation of the even subbands, i.e. when the subband splitting in the wire center is maximal.

Conclusion. We demonstrate that the spin DFT and the HF approaches provide qualitatively (and in most cases quantitatively) same description of a split-gate quantum wire in the IQH regime. This includes the electron density, spin polarization and the effective g factor. The both approach give the same values of the magnetic fields corresponding to the successive subband depopulation and qualitatively similar evolution of the magnetosubbands. Quantitatively, however, the HF and the DFT subbands are different (even though the corresponding total electron densities are practically the same). In contrast to the HF approach, the DFT calculations predict much larger spatial spin separation near the wire edge for the low fields (when the compressible strips for spinless electrons are not formed yet).

¹ G. F. Giuliani and G. Vignale, *Quantum Theory of the Electron Liquid*, (Cambridge University Press, Cambridge, 2005).
² J. M. Kinaret and P. A. Lee, Phys. Rev. B **42** 11768 (1990).
³ J. Dempsey, B. Y. Gelfand, and B. I. Halperin, Phys. Rev. Lett. **70**, 3639 (1993).
⁴ Y. Tokura and S. Tarucha, Phys. Rev. B **50**, 10981 (1994).
⁵ A. Manolescu and R. R. Gerhardts, Phys. Rev. B **51**, 1703 (1995).
⁶ O. Heinonen, M. I. Lubin, and M. D. Johnson, Phys. Rev. Lett. **75**, 4110 (1995); M. Ferconi, M. R. Geller, and G. Vignale, Phys. Rev. B **52**, 16357 (1995).
⁷ T. H. Stoof and G. E. W. Bauer, Phys. Rev. B **52**, 12143 (1995).
⁸ O. G. Balev and P. Vasilopoulos, Phys. Rev. B **56**, 6748 (1997).
⁹ A. Brataas, V. Gudmundsson, A. G. Mal'shukov, and K. A. Chao, J. Phys.: Condens. Matter **10**, 4267 (1998).
¹⁰ Z. Zhang and P. Vasilopoulos, Phys. Rev. B **66**, 205322

(2002).
¹¹ O. G. Balev, S. Silva, and N. Studart, Phys. Rev. B **72**, 085345 (2005).
¹² A. Struck, S. Mohammadi, S. Kettemann, and B. Kramer, Phys. Rev. B **72**, 245317 (2005).
¹³ S. Ihnatsenka and I. V. Zozoulenko, Phys. Rev. B **73**, 075331 (2006).
¹⁴ S. Ihnatsenka and I. V. Zozoulenko, Phys. Rev. B **73**, 155314 (2006).
¹⁵ S. Ihnatsenka and I. V. Zozoulenko, Phys. Rev. B **74** 075320 (2006); *ibid.*, **75** 035318 (2007).
¹⁶ for a review see, S. M. Reimann and M. Manninen, Rev. Mod. Phys. **74**, 1283 (2002).
¹⁷ see e.g. F. Evers, F. Weigend, and M. Koentopp, Phys. Rev. B **69**, 235411 (2004); C. Toher, A. Filippetti, S. Sanvito, and K. Burke, Phys. Rev. Lett. **95**, 146402 (2005); S. Ihnatsenka and I. V. Zozoulenko, Phys. Rev. B, in press (cond-mat/0703380).
¹⁸ B. Tanatar and D. M. Ceperley, Phys. Rev. B **39**, 5005,

- (1989).
- ¹⁹ D. B. Chklovskii, B. I. Shklovskii, and L. I. Glazman, Phys. Rev. B **46**, 4026 (1992); D. B. Chklovskii, K. A. Matveev, and B. I. Shklovskii, Phys. Rev. B **47**, 12605 (1993).
- ²⁰ T. Suzuki and T. Ando, J. Phys. Soc. Jpn. **62** 2986 (1993).
- ²¹ G. Muller, D. Weiss, K. von Klitzing, K. Ploog, H. Nickel, W. Schlapp, and R. Losch, Phys. Rev. B **46**, 4336 (1992).
- ²² M. Ciorga, M. Pioro-Ladriere, P. Zawadzki, P. Hawrylak, and S. A. Sachrajda, Appl. Phys. Lett. **80**, 2177 (2002).
- ²³ T. Ando, A. B. Fowler and F. Stern, Rev. Mod. Phys. **54**, 437 (1982).